MMSE BEAMFORMER BASED ON PARTIAL FFT DEMODULATION FOR OFDM UNDERWATER ACOUSTIC COMMUNICATIONS

Gema Piñero

Institute of Telecommunications
and Multimedia Applications
Universitat Politècnica de Valencia
Valencia, Spain
Email: gpinyero@iteam.upv.es

Andrew C. Singer

Coordinated Science Laboratory
University of Illinois at Urbana-Champaign
Urbana 61801, IL, USA
Email: acsinger@uiuc.edu

ABSTRACT

Underwater Acoustic (UWA) communications have to deal with channels that exhibit widely time-spreading multipath responses, together with Doppler spreading and limited bandwidth. These features seriously limit data throughput, even for sophisticated modulation schemes. Focusing on the large time-spreading characteristics, we analyze in this paper an OFDM UWA system such that the channel is longer than the Cyclic Prefix (CP) used. Under this condition, and considering an array of hydrophones at the receiver, we propose in this paper a Minimum Mean Square Error (MMSE) beamformer that makes use of two partial FFTs of half the original number of subcarriers to demodulate the OFDM signal. We show that one of the two demodulated signal can be received without Inter-Symbol Interference (ISI), even for longer-than-CP channels, and that the MMSE beamformer automatically is steered to direct and reflected paths obtaining an improvement of 4 dB in the Signal-to-Noise Ratio (SNR) and a reduction of 2 to 3 times the Bit Error Rate (BER) with respect to a conventional Delay-and-Sum (DS) beamformer.[1]

Index Terms— Underwater Acoustic Communications, broadband acoustic beamformer, OFDM.

I. INTRODUCTION

Underwater Acoustic (UWA) communication channels present a multipath model together with particular features not common to other wireless communications [1], [2]. They exhibit present time variations even when the transmitter and the receiver are anchored, due to the changing sea surface (waves), and the spatial variation of the propagation velocity which strongly depends on water temperature. Figure 1 shows signal propagation where the direct path is summed up with reflected paths due to multiple surface and seabed reflections. Propagation attenuation increases with frequency, resulting in near 5 dB/Km loss for a carrier frequency of 20 kHz or 12 dB/Km at 40 kHz, which limits the useful bandwidth to a few kHz. Although small compared to other communications systems, the bandwidth of the information signal is usually broadband compared to the carrier frequency.

[1]This work has been partially supported by Spanish Government through CYCIT grant TEC2009-13741 and Prog. Nac. Movilidad RRHH 2011, and by Regional Government through PROMETEO/2009/013.

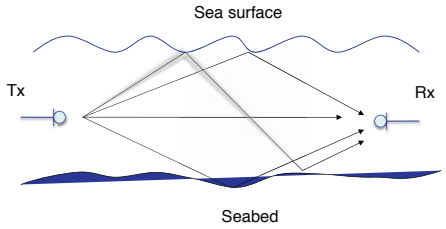

Fig. 1. Signal propagation through a multipath underwater acoustic channel.

Multipath in the UWA channel can be modeled as a time-varying channel impulse response $h(t,\tau)$. If the transmitter and receiver are stationary and the coherence time is large enough, i.e. $h(t,\tau) \simeq h(\tau)$, $h(\tau)$ is a linear time-invariant (LTI) multipath channel. Let us consider the equivalent discrete-time model of the received signal $y(t)$ when sampled with sample period $T_s = 1/f_s$. The received discrete-time signal can be expressed through the convolution sum between the transmitted signal and the multipath channel $y(n) = \sum_{l=0}^{L-1} h(l)x(n-l)$ where $y(n) = y(nT_s)$, $x(n) = x(nT_s)$, and L is the length, in number of symbols, of the discrete-time channel $h(n)$. The discrete-time model of the channel is useful for the design of the equalizer and detector at the receiver. While similar in form to Radio-Frequency multipath channels, UWA channels are widely spread in time. The large delay spread together with small bandwidth severely limits the throughput in these communication systems. A long-range UWA channel can exhibit a delay spread of 200-400 ms depending on the propagating environment [3]. Regarding the receiver complexity, extremely long channels require even longer equalizers, much more complex for the multi-channel case. One way to simplify the receiver is to use a beamformer in the first stage of the receiver, and to process the resulting signal through a Decision-Feedback Equalizer in a second stage [4], [5].

Regarding OFDM communications in UWA channels, Cyclic Prefix (CP) length should be longer than channel

delay spread to avoid Inter-Symbol Interference (ISI), which in turn requires large OFDM symbols in order to not sacrifice rate. Throughout this paper, we have focused our work on LTI UWA channels considering any Inter-Carrier Interference (ICI) due to motion negligible. While the CP length in OFDM communications has to be larger than channel length, long-range communications may be impractical due to the channel delay spread. However, if a CP shorter than the channel is used, the circular convolution property of the Discrete-Time Fourier (DFT) is no longer respected and the received signal is no longer the product of the original symbol and the channel DFT. We will model the use of shorter CP as a random error added to each subcarrier, as we will show in Section II.

Using this OFDM signal and error model, we will design a Minimum Mean Square Error (MMSE) beamformer that makes use of two DFTs of half the number of subcarriers. We will study the error model for this particular design when channel time-spreading is larger than the CP. Finally, we will compare the use of the MMSE beamformer with the conventional Delay-and-Sum (DS) beamformer [6] by means of numerical simulations.

II. PARTIAL FFT DEMODULATION OF THE OFDM RECEIVED SIGNAL

Let us consider a single channel UWA communication system transmitting linear modulated symbols through OFDM. Once the inverse DFT of the baseband modulated symbols $X(k)$ is performed, a Cyclic Prefix (CP) formed by the last $L_{\rm CP}$ samples of $x(n) = {\rm DFT}^{-1}[X(k)]$ is added to form $x_{\rm CP}(n)$. In absence of noise and interference, the received signal $y_{\rm CP}(n)$ can be expressed as:

$$y_{\rm CP}(n) = x_{\rm CP}(n) * h(n) = \sum_{l=0}^{L-1} h(l) x_{\rm CP}(n-l) \quad (1)$$

The last N samples of $y_{\rm CP}(n)$ correspond to the circular convolution between $x(n)$ and $h(n)$ denoted by $x(n) \,\textcircled{\scriptsize N}\, h(n)$. The DFT of the circular convolution of two signals is equal to the multiplication of their respective DFTs, which means that symbols $X(k)$ are multiplied by the complex amplitude of the corresponding subcarriers:

$$y(n) = h(n) \,\textcircled{\scriptsize N}\, x(n) \overset{\rm DFT}{\longleftrightarrow} Y(k) = H(k)X(k) \quad (2)$$

where $Y(k)$ is the DFT of the last N samples of $y_{\rm CP}(n)$, denoted by $y(n)$.

The use of a DFT that processes separately small sets of subcarriers to improve Doppler selectivity has been recently proposed in [7]. It has been shown to be computationally inexpensive, and it presents good performance for DFTs of $N/4$ and $N/8$ points, N being the total number of subcarriers of the OFDM symbol. In our study, Doppler selectivity is considered to have been compensated in a previous stage (by resampling the signal as, for example, in [8]), and our study has focused on the use of DFTs of $N/2$ points to improve the Signal-to-Noise Ratio (SNR) and Bit Error Rate (BER) in longer-than-CP channels.

Let us define two sequences of $N/2$ points $x_1(n)$ and $x_2(n)$ obtained from $x(n)$ as:

$$x_1(n) = x(n)\ ,\ n = 0, \ldots, N/2-1 \quad (3)$$
$$x_2(n) = x(n+N/2)\ ,\ n = 0, \ldots, N/2-1 \quad (4)$$

that is, $x_1(n)$ is formed by the first $N/2$ points of OFDM sequence $x(n)$ and $x_2(n)$ is formed by the last $N/2$ points. Consider now the definition of two similar sequences over the received OFDM signal $y(n)$ once the CP has been dropped, that is, $y_1(n) = y(n)\,,\ n = 0, \ldots, N/2-1$ and $y_2(n) = y(n+N/2)\,,\ n = 0, \ldots, N/2-1$.

Given the expressions of $x_1(n)$ and $x_2(n)$ in (3)-(4), signal $x_1(n)$ can be considered as an OFDM signal whose prefix is formed by the last $L_{\rm CP}$ samples of $x_2(n)$, whereas signal $x_2(n)$ is considered to have a prefix formed by the last $L_{\rm CP}$ samples of $x_1(n)$.

One way to constrain $x_1(n)$ and $x_2(n)$ to fulfill the circular convolution property is to use a particular pilot sequence $X(k)$ such that its inverse DFT holds $x_1(n) = x_2(n)$. This implies that $X(k) = {\rm DFT}[x(n)]$ must be null at odd values of k. Assuming that $x_1(n) = x_2(n)$, equations (5)-(7) summarize the different relationships between sequences and their corresponding DFTs, considering in all sequences a CP larger or equal to the channel length ($L_{\rm CP} \geqslant L$):

$$y(n) = x(n) \,\textcircled{\scriptsize N}\, h(n) \overset{\rm DFT}{\longleftrightarrow} Y(k) = X(k)H_{\rm N}(k) \quad (5)$$
$$y_1(n) = x_1(n) \,\textcircled{\scriptsize N/2}\, h(n) \overset{\rm DFT}{\longleftrightarrow} Y_1(k) = X_1(k)H_{\frac{\rm N}{2}}(k) \quad (6)$$
$$y_2(n) = x_2(n) \,\textcircled{\scriptsize N/2}\, h(n) \overset{\rm DFT}{\longleftrightarrow} Y_2(k) = X_2(k)H_{\frac{\rm N}{2}}(k) \quad (7)$$

where $X_1(k) = {\rm DFT}[x_1(n)]$, $X_2(k) = {\rm DFT}[x_2(n)]$, $H_{\rm N}(k)$ is the DFT of N points of $h(n)$, and $H_{\frac{\rm N}{2}}(k)$ is the corresponding DFT of $N/2$ points of $h(n)$. Both DFTs are related through $H_{\frac{\rm N}{2}}(k) = H_{\rm N}(2k)\,,\ k = 0, 1, \ldots N/2-1$, as long as $L < N/2$. It can be stated that $y_1(n)$ and $y_2(n)$ are the respective circular convolution of $x_1(n)$ and $x_2(n)$ with channel $h(n)$.

In the case of channels spreading further than the CP but less than $N/2$, that is, $L_{\rm CP} < L$ and $L < N/2$, the last N samples of the received sequence $y_{\rm CP}(n)$ given by (1) no longer represent the circular convolution between $x(n)$ and $h(n)$: the first $L-1-L_{\rm CP}$ samples of $y(n)$ are different from the corresponding ones of $h(n) \,\textcircled{\scriptsize N}\, x(n)$, whereas the last $N-(L-1-L_{\rm CP})$ are equal. The same effect can be observed on $y_1(n)$. However $y_2(n)$ does fulfill the property in (7) because the cyclic prefix of $x_2(n)$ is formed by sequence $x_1(n)$ and extends over $N/2$. Therefore, $y_2(n)$ can be expressed as in (7), whereas $y_1(n)$ is given

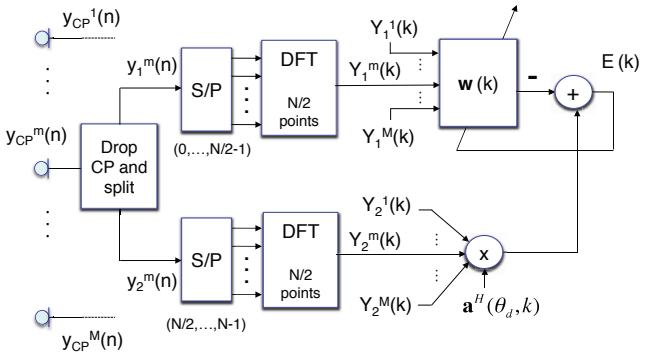

Fig. 2. Block diagram of the MMSE beamforming.

by $y_1(n) = x_1(n) \textcircled{N} h(n) + q(n)$ where $q(n)$ is an error sequence of length $L-1-L_{\mathrm{CP}}$. In fact, $q(n)$ is the Inter-Symbol Interference (ISI) produced by the multipath channel that is not cancelled because of $L > L_{\mathrm{CP}}$.

The corresponding DFT of $y_1(n)$ can then be expressed as:

$$Y_1(k) = X_1(k)H_{\frac{\mathrm{N}}{2}}(k) + Q(k) \tag{8}$$

where $Q(k)$ is the DFT of $N/2$ points of the sequence $q(n)$. It has to be noted that the ISI error $q(n)$ is confined to the first $L-1-L_{\mathrm{CP}}$ samples in time, whereas $Q(k)$ is spread over all frequencies from $k=0$ to $k=N/2-1$. In the next section we will make use of the different expressions of $Y_1(k)$ and $Y_2(k)$ to design an MMSE beamformer at the receiver avoiding the requirement of knowing the angles of arrival of the multiple paths.

III. MINIMUM MEAN SQUARED ERROR (MMSE) BEAMFORMER BASED ON PARTIAL FFT

In Section II, the model of a single OFDM-UWA channel has been stated. We introduce now a multi-channel communication system that makes use of multiple hydrophones at the receiver. From Figure 1, it can be assumed that different paths arrive to the hydrophone array from different angles, called Directions-of-Arrival (DoA), and are denoted by θ. The DoA is defined as the angle of arrival with respect to the line of the hydrophones for a linear array.

Let us assume that a coarse estimate of the DoA of the direct path in Figure 1 is calculated (for example, by means of 2-D frequency-θ spectral estimation of the received data), and denote that direction as θ_d. The block diagram of the proposed scheme is depicted in Figure 2 where $\mathbf{a}(\theta_d, k)$ is the steering vector [6] for DoA θ_d and frequency k, and a linear array of M hydrophones has been considered. The M components of the steering vector $\mathbf{a}(\theta_d, k)$ depend on the array geometry, the nominal frequency, the propagation velocity, and on θ_d.

Signal y_{CP}^m is the signal recorded at the m-th hydrophone such that (1):

$$y_{\mathrm{CP}}^m = x_{\mathrm{CP}} * h^m(n) + v^m(n) \tag{9}$$

where $v^m(n)$ is an additive complex white Gaussian noise of zero mean and variance σ_n^2, and $h^m(n)$ is the channel impulse response between the transmitter and the m-th hydrophone.

As it can be seen from Figure 2, signals y_{CP}^m are reduced to their last N samples by dropping the Cyclic Prefix. They are subsequently split in two to compute two partial DFTs of $N/2$ points obtaining sequences $Y_1^m(k)$ and $Y_2^m(k)$, for $k = 1, \ldots, N/2$. From this point on, hydrophone outputs are collected together at each k in order to form the following spatial vectors:

$$\mathbf{Y}_i(k) = \left[Y_i^1(k), \ldots, Y_i^m(k), \ldots, Y_i^M(k)\right]^T \quad i = 1, 2 \tag{10}$$

where superscript $(\cdot)^T$ stands for transposed.

Then, $\mathbf{a}^H(\theta_d, k)\mathbf{Y}_2(k)$ is used as the reference signal, whereas $\mathbf{Y}_1(k)$ is filtered by the narrowband beamformer, $\mathbf{w}(k) = [w^1(k), \ldots, w^m(k), \ldots, w^M(k)]^T$. The MMSE beamformer of Figure 2 for frequency k can be expressed as :

$$\mathbf{w}_{\mathrm{MMSE}}(k) = \min_{\mathbf{w}} \mathbb{E}[|E(k)|^2] \tag{11}$$

where $E(k)$ is the error signal formed as:

$$E(k) = \mathbf{a}^H(\theta_d, k)\mathbf{Y}_2(k) - \mathbf{w}^H(k)\mathbf{Y}_1(k) \tag{12}$$

where superscript $(\cdot)^H$ stands for transposed and conjugated.

Substituting equation (12) into (11), the MMSE weights can be calculated as:

$$\mathbf{w}_{\mathrm{MMSE}}(k) = \mathbf{R}_{\mathrm{Y}_1}^{-1}(k)\mathbf{R}_{\mathrm{Y}_1\mathrm{Y}_2}(k)\mathbf{a}(\theta_d, k) \tag{13}$$

where $\mathbf{R}_{\mathrm{Y}_1}(k)$ is the autocorrelation matrix of vector $\mathbf{Y}_1(k)$ and $\mathbf{R}_{\mathrm{Y}_1\mathrm{Y}_2}(k)$ is the correlation matrix between vectors $\mathbf{Y}_1(k)$ and $\mathbf{Y}_2(k)$. Both matrices can be estimated from a number $N_T \geqslant M$ of respective snapshots assuming stationary signals within a period $N_T \cdot N \cdot T_s$ seconds. The general expression of the estimated correlation matrix for column vectors $\mathbf{Y}_i(k), \mathbf{Y}_j(k)$ is given by:

$$\widehat{\mathbf{R}}_{\mathrm{Y}_i\mathrm{Y}_j}(k) = \frac{1}{N_T}\sum_{n=1}^{N_T} \mathbf{Y}_i^{(n)}(k)\mathbf{Y}_j^{(n)}(k)^H \tag{14}$$

where $\mathbf{Y}^{(n)}(k)$ denotes the spatial vector formed by k-th DFT coefficients calculated from the OFDM symbol presented at the hydrophones at time n.

Considering now the models of $Y_1(k)$ and $Y_2(k)$ given in (8) and (7) respectively, and assuming that pilot signals $X_1(k) = X_2(k)$ have unit variance and are uncorrelated with all the noise signals $V_1^m(k)$ and $V_2^m(k)$, and with error $Q(k)$, the MMSE beamformer (13) is formed by the following terms:

$$\mathbf{w}_{\mathrm{MMSE}} = \left(\mathbf{R}_{\mathrm{H}} + \mathbf{R}_{\mathrm{V_1}} + \mathbf{R}_{\mathrm{Q}}\right)^{-1} \mathbf{R}_{\mathrm{H}} \mathbf{a}(\theta_d) \qquad (15)$$

where $\mathbf{R}_H = \mathbb{E}[\mathbf{H}(k)\mathbf{H}^H(k)]$ is the autocorrelation matrix of the channel spatial vector, whose components are the channel values at each hydrophone, $\mathbf{H}(k) = [H^1(k), \ldots, H^M(k)]^T$. $\mathbf{R}_{\mathrm{V_1}}$ is the autocorrelation matrix of noise spatial vector $\mathbf{V}_1(k) = [V_1^1(k), \ldots, V_1^M(k)]^T$, and $\mathbf{R}_{\mathrm{Q}}$ is the autocorrelation matrix of spatial error vector due to ISI, $\mathbf{Q}(k)$. The MMSE beamformer minimizes the difference between the reference signal, $\mathbf{a}^H(\theta_d, k)\mathbf{Y}_2(k)$ and the beamformer output. As the main difference between both signals is due to the noise and the ISI $\mathbf{Q}(k)$, the resulting beamformer will try to reduce both contributions.

To better understand its behavior, let us assume a simple UWA channel with only direct and reflected paths, denoted by $h_d(n)$ and $h_r(n)$ respectively. Thus, spatial channel vector can be expressed as $\mathbf{H} = \mathbf{a}(\theta_d)H_d + \mathbf{a}(\theta_r)H_r$, where the dependence on k has been dropped for the sake of clarity. As H_d and H_r can be assumed uncorrelated, the autocorrelation matrix of $\mathbf{H}$ can be expressed as:

$$\mathbf{R}_{\mathrm{H}} = \mathbb{E}[|H_d|^2]\mathbf{a}(\theta_d)\mathbf{a}^H(\theta_d) + \mathbb{E}[|H_r|^2]\mathbf{a}(\theta_r)\mathbf{a}^H(\theta_r) \quad (16)$$

Substituting (16) into the last term of (15) we obtain:

$$\mathbf{R}_{\mathrm{H}}\mathbf{a}(\theta_d) = M\mathbb{E}[|H_d|^2]\mathbf{a}(\theta_d) + \alpha M\mathbb{E}[|H_r|^2]\mathbf{a}(\theta_r), \quad (17)$$

where $\mathbf{a}^H(\theta_d)\mathbf{a}(\theta_d) = M$ and $\alpha = \mathbf{a}^H(\theta_r)\mathbf{a}(\theta_d)/M$ is a complex scalar such that $|\alpha| \leqslant 1$. Substituting (17) in (15), the MMSE beamformer can be expressed as:

$$\begin{aligned} \mathbf{w}_{\mathrm{MMSE}} &= M\left(\mathbf{R}_{\mathrm{H}} + \mathbf{R}_{\mathrm{V_1}} + \mathbf{R}_{\mathrm{Q}}\right)^{-1}\left[\mathbb{E}[|H_d|^2]\mathbf{a}(\theta_d) + \right. \\ &+ \left. \alpha\mathbb{E}[|H_r|^2]\mathbf{a}(\theta_r)\right] \qquad (18) \end{aligned}$$

The statistical analysis of MMSE beamformer is out of the scope of this paper, but from expression (18) it can be seen that MMSE beamformer has a direct dependence on both direct and reflected paths, avoiding a wrong performance when dealing with multipath (correlated) signals.

IV. NUMERICAL SIMULATIONS

In this section the performance of the proposed MMSE beamformer for a multichannel UWA OFDM communication system that makes use of N=512 subcarriers is evaluated. The channel is composed of three different diffuse paths (similar to the plot of Figure 1), a direct signal arriving from $\theta_d = 90°$ and spreading from $\tau = 0 \cdot T_{\mathrm{sym}}$ to $\tau = 7 \cdot T_{\mathrm{sym}}$, a first reflected signal arriving from $\theta_{r1} = 115°$ and spreading in time from $\tau = 6 \cdot T_{\mathrm{sym}}$ to $\tau = L \cdot T_{\mathrm{sym}}$, and a second reflected signal arriving from $\theta_{r2} = 45°$ and spreading in time from $\tau = 16 \cdot T_{\mathrm{sym}}$ to $\tau = L \cdot T_{\mathrm{sym}}$, where L is the total length of the channel in symbols and T_{sym} is the PSK symbol period. Channel length varies in the range $L \subseteq (32, 54) \cdot T_{\mathrm{sym}}$. Notice that both reflected paths are simulated to be of length L, since, in a realistic environment, usually both seabed and wave reflections cause symbol time-spreading. Direct and reflected paths have individual taps $h(\tau)$ modeled as independent complex Gaussian of zero mean and unit variance at $\tau = l \cdot T_{\mathrm{sym}}$.

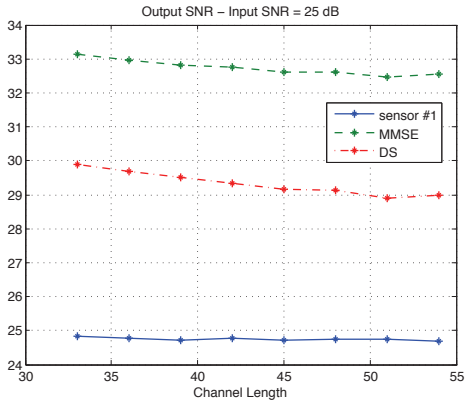

Fig. 3. SNR for the first hydrophone (without beamforming), and after MMSE and DS beamforming. Units are in dB.

A source of BPSK pilot symbols $X(k)$ such that $x_1(n) = x_2(n)$ is transmitted using OFDM with a fixed Cyclic Prefix length of 32 symbols. The pilot sequence is used as a probe to initially steer the beamformers. A linear array of $M = 10$ hydrophones with half wavelength spacing has been used and white Gaussian noise has been added at each hydrophone resulting in a received SNR of 25 dB. Finally, MMSE beamformer of Section III and Delay-and-Sum (DS) beamformer given by $\mathbf{w}_{\mathrm{DS}}(k) = \mathbf{a}^H(\theta_d, k)$ have been calculated for 300 independent runs.

Figure 3 shows the output SNR for the first hydrophone (without beamformer) and after MMSE and DS beamforming respectively. It can be seen that the SNR obtained by the MMSE is 3-4 dB higher than DS and 8 dB higher than input SNR (first sensor) for the whole range of channel lengths L. This behavior agrees with the Array Gain (AG) expected for an array of 10 sensors separated $d = \lambda/2$ [3], once the SNR has been maximized.

Another interesting feature is the capacity of the beamformer to reduce the contribution of the channel components outside the CP. Figure 4 shows the energy ratio between channel taps allocated outside the CP and those placed within the CP for filtered MMSE and DS channels and for the channel seen at the first hydrophone. DS decreases this ratio in 2 dB and MMSE only in 1 dB, but considering that reflected paths produce all the outside-CP energy, and that MMSE has a significant increase in SNR due to their contributions, it can be stated that MMSE is actually decreasing the energy placed outside CP with respect to the original channel.

Finally, the Bit Error Rate (BER) has been calculated for 100 independent runs. For each run, $2.5 \cdot 10^4$ uncoded

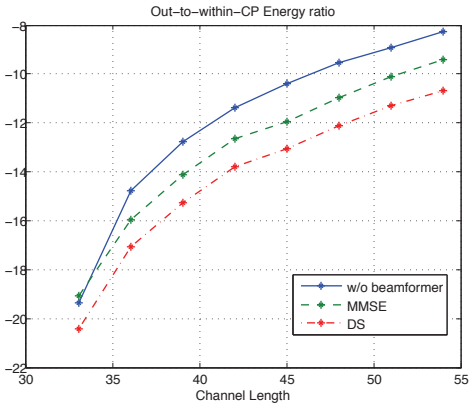

Fig. 4. Energy ratio between channel taps outside the CP and those placed within the CP: original (first hydrophone) and after MMSE and DS beamforming. Units are in dB.

bits have been mapped into QPSK symbols and have been transmitted by means of 26 OFDM symbols. For all symbols, 20 subcarriers at each side have not been used forming a guard band of null content. Previously, a probe formed by 12 pilot OFDM symbols has been used to design the MMSE beamformer. From the probe, estimated channel coefficients $\hat{H}(k)$ have been calculated for MMSE and DS filtered signals, and for the signal received at the first hydrophone as well. As the pilot sequence is such that $X(k) = 0$ for odd frequencies, estimated coefficients $\hat{H}(k)$ have been directly obtained only for even k. Afterwards, coefficients $\hat{H}(k)$ for odd k have been calculated through linear interpolation. Figure 5 shows the BER obtained for two different channel lengths, $L = 35$ and $L = 50$. Both figures show a reduction of the BER when using MMSE instead of DS beamforming, achieving a significant decrease of 3-4 times for high SNRs.

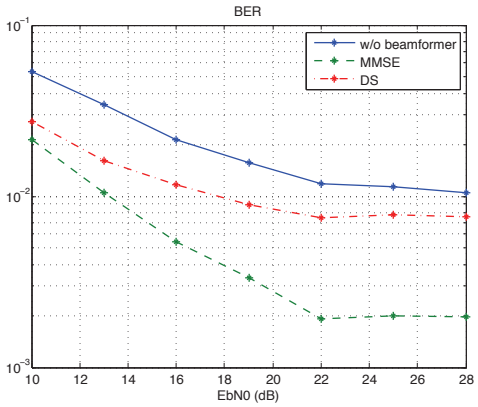

(a) Channel length, $L = 35$

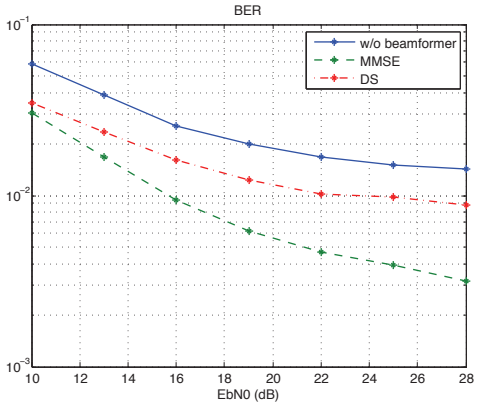

(b) Channel length, $L = 50$

Fig. 5. BER obtained for OFDM modulated QPSK symbols and different channel lengths. Equal CP length of $L_{\mathrm{CP}} = 32$ symbols has been used for both channels.

V. CONCLUSION

An MMSE beamformer based on two partial DFTs of $N/2$ subcarriers has been proposed for improving the received SNR and BER when dealing with widely time-spreading UWA channels. A simple analysis for one direct and one reflected path have shown that MMSE beamformer is automatically steered to both DoAs, whereas conventional DS only enhances the direct path. Numerical simulations have confirmed this benefit obtaining BER reductions of 2 to 4 times depending on the received SNR and the channel length.

VI. REFERENCES

[1] M. Stojanovic and J. Preisig, "Underwater acoustic communication channels: Propagation models and statistical characterization," *Communications Magazine, IEEE*, vol. 47, no. 1, pp. 84 –89, January 2009.

[2] A. Singer, J. Nelson, and S. Kozat, "Signal processing for underwater acoustic communications," *Communications Magazine, IEEE*, vol. 47, no. 1, pp. 90 –96, January 2009.

[3] T. Yang, "A study of spatial processing gain in underwater acoustic communications," *Oceanic Engineering, IEEE Journal of*, vol. 32, no. 3, pp. 689 –709, july 2007.

[4] M. Stojanovic, J. Catipovic, and J. Proakis, "Reduced-complexity simultaneous beamforming and equalization for underwater acoustic communications," in *OCEANS '93. Engineering in Harmony with Ocean. Proceedings*, oct 1993, pp. III426 –III431 vol.3.

[5] P.-P. Beaujean and L. LeBlanc, "Adaptive array processing for high-speed acoustic communication in shallow water," *Oceanic Engineering, IEEE Journal of*, vol. 29, no. 3, pp. 807 – 823, july 2004.

[6] D. H. Johnson and D. E. Dudgeon, *Array signal processing: Concepts and techniques*. Prentice-Hall, Signal Processing Series, 1993.

[7] S. Yerramalli, M. Stojanovic, and U. Mitra, "Partial fft demodulation: A detection method for doppler distorted ofdm systems," in *Signal Processing Advances in Wireless Communications (SPAWC), 2010 IEEE Eleventh International Workshop on*, June 2010, pp. 1 –5.

[8] L. Baosheng, Z. Shengli, M. Stojanovic, L. Freitag, and P. Willett, "Non-uniform doppler compensation for zero-padded ofdm over fast-varying underwater acoustic channels," in *OCEANS 2007 - Europe*, June 2007, pp. 1 –6.